Ferdowsi University of Mashhad

I C C K E

International Conference on Computer and Knowledge Engineering

CERTIFICATE OF PRESENTATION

It is certified that

Mohammad-Bagher Khamehchian Mahdi Saadatmand-Tarzjan

Presented a paper titled

A New Pacth-Based Active Contour for Segmentation of the Myocardium of the Left Ventricle in Cardiac Magnetic Resonace Images

during the 3rd International Conference on Computer and Knowledge Engineering (ICCKE 2013), held on 31 October & 1 November 2013 at Ferdowsi University of Mashhad

Mohsen Kahani, PhD

ICCKE 2013 Conference Chair

ICCKE Secretariat, Faculty of Engineering, Ferdowsi University of Mashhad, Azadi Square, Mashhad, Iran

Website: http://iccke.um.ac.ir **Email: iccke@um.ac.ir**

A New Patch-Based Active Contour for Segmentation of the Myocardium of the Left Ventricle in Cardiac Magnetic Resonance Images

M.-B. Khamechain
Department of Electrical Engineering
Ferdowsi University of Mashhad
P.O.Box 91775-1111 Mashhad, Iran
bagher.m.kh@gmail.com

M. Saadatmand-Tarzjan
Department of Electrical Engineering
Ferdowsi University of Mashhad
P.O.Box 91775-1111 Mashhad, Iran
saadatmand@um.ac.ir

***Abstract*— In this paper, a geometric active contour for segmentation of the myocardium of the left ventricle in cardiac magnetic resonance (CMR) images is presented. The stochastic active contour scheme (STACS) and its variants, such as Li's method [12], are well-known frequently-used approaches for segmentation of the myocardium boundaries. However, they have significant difficulties with the image inhomogeneity due to using a region-based energy term established on the global Gaussian probability density function. It seems that localizing the region-based term of the energy functional is an effective solution to tackle the above problem. We enhance Li's method by substituting the region-based terms of endocard and epicard active contours with those of the local binary fitting (LBF) and local Gaussian distribution fitting (LGDF), respectively. Both LBF and LGDF belong to the category of patch-based active contours which can essentially handle the image inhomogeneity. Experimental results demonstrated that the proposed method provides significantly superior performance compared to Li's method in segmentation of the myocardium of the left ventricle.**

Keywords: Myocardium Segmentation; Geometric Active Contour; Level-Set; LBF; LGDF

I. INTRODUCTION

Investigation of myocardium of the left ventricle eventuates to diagnosis of some cardiac dysfunction, such as cardiomyopathy and ischemia. These diseases, which suffer the abnormal thickness of the myocardium due to infection or narrowing of coronary arteries, can be diagnosed by processing of cardiac images [1]. The cardiac magnetic resonance (CMR) imaging presents precise spatial and temporal information from the heart muscles. More precisely, CMR imaging provides a number of multisection-multiphase CMR images in the heart short-axis which include suitable information about different heart cavities and muscles during the cardiac cycle. In the traditional approach, the myocardium is manually delineated by a radiologist/cardiologist expert to detect the endocard and epicard (endo-epicard) boundaries of the left ventricle. However, it is too time-consuming and suffers from different experts' insights. A number of researchers address the above problem by computer-based processing of CMR images [2]. Active contours are most well-known and frequently-used methods for CMR image segmentation [3,4]. Generally speaking, active contours are deformable models which can deform/evolve in the image domain to minimize the internal and external energies. The internal energy makes the curve smooth, while the external energy moves it toward the interested features in the image domain. For example, Lynch *et al* [5] proposed two coupled active contours for segmentation of the endo-epicard boundaries of the left ventricle. They employed the geodesic active contour (GAC) [6] with statistical a priori shape information. Also, Woo *et al* [7] took advantage of GAC and active contour without edge [8] with a coupling region-based energy term based on a priori shape information.

Pluempitiwiriyawej *et al* [9] proposed the stochastic active contour scheme (STACS) in which the energy functional includes three different terms for taking account of the region, edge, and shape information in order to segment the endocad-boundary of the left ventricle. However, STACS provides acceptable results, only when used with low-contrast CMR images [10], due to employing Gaussian distributions of the region-based energy term [11].

Chen *et al* [11] improved STACS by using a non-parametric non-Gaussian region-based model. They successfully used the suggested method for segmentation of myocardial boundaries in cine-displacement-encoded MR images.

In another work, Li *et al* [12] proposed an elegant method to address STACS troubles with the Gaussian distribution of the region-based energy term. They coupled two modified STACS to simultaneously segment endo-epicard boundaries. In more detail, both the outer and inner regions of the endocard and epicard active contours were limited to the myocardium region. Besides, the outer region of the epicard active contour is divided into two brighter and darker areas. For each area a separate Gaussian distribution is employed to enhance the region-based term of STACS. For stricter coupling, the epicard active contour attempts to keep constant average distance to the endocard active contour during deformation. Despite some remarkable results, Li's method may fail to extract epicard boundary in significantly inhomogeneous CMR images.

Indeed, Li's method divides the image domain into some sub-regions for localizing the Gaussian distribution of the region-based energy term. However, it is not usually sufficient for extremely inhomogeneous CMR images. In this paper, we enhance the performance of Li's method by substituting the region-based terms of endocard and epicard energy functionals with two new patch-based local models inspired by local binary fitting (LBF) [13] and

local Gaussian distribution fitting (LGDF) [14], respectively. In more detail, LBF takes advantage of the local intensity mean to cope intensity inhomogeneity. However in the presence of extremely inhomogeneous regions, it is necessary to take account of the local intensity variance as well. This problem is effectively addressed by LGDF.

The paper is organized as follows. In the next section, we briefly explain Li's method. LBF and LGDF are stated in Section III. Section IV is devoted to state the proposed method in detail. Experimental results are presented in Section V and finally, conclusions are drawn in Section VI.

II. LI'S MODEL

The energy functional of STACS is originally composed of four terms:

$$J(\phi) = \lambda_1 J_1(\phi) + \lambda_2 J_2(\phi) + \lambda_3 J_3(\phi) + \lambda_4 J_4(\phi) \tag{1}$$

where ϕ is the level-set function and $J_1(\phi)$, $J_2(\phi)$, $J_3(\phi)$, and $J_4(\phi)$ represent the region-based, edge-based, a priori-shape based, and regulator terms of the energy functional, respectively. Furthermore, λ_1, λ_2, λ_3, and λ_4 denote the weighting coefficients of the above terms, correspondingly. They are automatically adjusted in terms of the number of iterations during the deformation process of the active contour.

In more detail, the region-based term, $J_1(\phi)$, is consist of two distinct Gaussian probability density functions (PDFs), corresponding to the intensity distributions of the background (outside) and foreground (inside) pixels of the active contour, respectively, as follows:

$$\begin{aligned} J_1(\phi) = \int_\Omega & -\ln\left[p_1(u(x,y))\right] H(\phi(x,y)) \\ & -\ln\left[p_2(u(x,y))\right][1 - H(\phi(x,y))]\, dxdy \end{aligned} \tag{2}$$

where $u(x, y)$ and Ω represent the CMR image and its domain, respectively. Also, p_1 and p_2 are Gaussian PDFs of the background and foreground, correspondingly, and $H_\varepsilon(\phi)$ denotes a regularized Heaviside function given by:

$$H_\varepsilon(\phi) = \frac{1}{2}\left(1 + \frac{2}{\pi}\arctan(\frac{\phi}{\varepsilon})\right) \tag{3}$$

By using the Euler-Lagrange equation, STACS evolution equation is obtained as [10]:

$$\frac{\partial \phi}{\partial t} = \left[\lambda_1 (M_1 - M_2) - A(\phi, t)\right]\delta(\phi) \tag{4}$$

where $A(\phi, t)$ includes the terms of the Euler-Lagrange equation equivalent to the last three terms of the energy functional (for more details, see [10]), $\delta(\phi)$ is the derivative of $H(\phi)$ and M_k are computed by:

$$M_k = \frac{1}{2}\ln(2\pi\sigma_k^2) + \frac{(u(x,y) - m_k)^2}{2\sigma_k^2} \qquad k = 1,2 \tag{5}$$

where m_k and σ_k are the intensity average and variance, respectively, for the foreground (k=1) and background (k=2) regions.

Li *et al* [12] extended STACS energy functional by jointing two distinct modified STACSs for simultaneous segmentation the endo-epicard boundaries. In more detail, they further localized the energy functional by limitation of the definition domain of the Gaussian PDFs. More precisely, both p_2 and p_1 of the endocard and epicard active contours, respectively, are defined only on the domain of the myocardium region (between the endocard and epicard active contours). Furthermore, in the epicard active contour, instead of p_2, two distinct Gaussian PDFs are separately defined for the darker and brighter areas of the background.

Besides, the coupling term $J_5(\phi_2)$ is added to the epicard energy functional to keep constant average distance to the endocard active contour (m) during deformation:

$$J_5(\phi_2) = \int_\Omega D\ \left[H_\varepsilon(D) - H_\varepsilon(\phi_2)\right] dxdy \tag{6}$$

where the distance function D is equal to ϕ_2+m and ϕ_2 is the level set of the epicard active contour (for more details, see [12]).

III. PATCH-BASED ACTIVE CONTOURS

As previously stated, Li's method could partially tackle STACS shortcomings by localizing the region-based term of the energy functional. On the other hand, patch-based active contours such as LBF [13] and LGDF [14] effectively handle the image inhomogeneity problem by using the local kernel function in the energy functional [13-18]. Hence, it is worth to explain LBF and LGDF (as two well-known frequently-used examples of patch-based of active contours) in more detail.

A. Local Binary Fitting (LBF)

The energy functional of LBF is given by [13]:

$$\begin{aligned} & J_{LBF}(\phi, f_1, f_2) = \\ & \alpha_1 \int_\Omega \int K_\sigma(\boldsymbol{x} - \boldsymbol{y}) \left|u(\boldsymbol{y}) - f_1(\boldsymbol{x})\right|^2 M_{1,\varepsilon}(\phi(\boldsymbol{y}))\, d\boldsymbol{y} d\boldsymbol{x} + \\ & \alpha_2 \int_\Omega \int K_\sigma(\boldsymbol{x} - \boldsymbol{y}) \left|u(\boldsymbol{y}) - f_2(\boldsymbol{x})\right|^2 M_{2,\varepsilon}(\phi(\boldsymbol{y}))\, d\boldsymbol{y} d\boldsymbol{x} + \\ & \int_\Omega B(H, \phi, \boldsymbol{x})\, d\mathrm{x} \end{aligned} \tag{7}$$

where $\boldsymbol{y}$ represents the neighbors of the center pixel $\boldsymbol{x}$ and α_1 and α_2 are two constant coefficients. Also, we have:

$$\begin{cases} M_{\varepsilon,1}(\phi(\boldsymbol{y})) = H_\varepsilon(\phi(\boldsymbol{y})) \\ M_{\varepsilon,2}(\phi(\boldsymbol{y})) = 1 - H_\varepsilon(\phi(\boldsymbol{y})) \end{cases} \tag{8}$$

and K_σ is the Gaussian kernel (with STD of $\sigma > 0$), computed by:

$$K_\sigma(\boldsymbol{u}) = \frac{1}{(2\pi)^{n/2}\sigma^n} e^{-|\boldsymbol{u}|^2 / 2\sigma^2} \tag{9}$$

The functions $f_1(\boldsymbol{x})$ and $f_2(\boldsymbol{x})$ locally approximate $u(\boldsymbol{x})$ in the regions inside and outside of the active contour, respectively. They can be optimally computed by:

$$f_i(\boldsymbol{x}) = \frac{K_\sigma(\boldsymbol{x}) * \left[M_{\varepsilon,i}(\phi(\boldsymbol{x}))u(\boldsymbol{x})\right]}{K_\sigma(\boldsymbol{x}) * M_{\varepsilon,i}(\phi(\boldsymbol{x}))} \qquad i = 1,2 \tag{10}$$

The first two terms of (7) move the active contour toward the desired boundary while the last expression $B(H,\phi,\boldsymbol{x})$ includes some regulation terms to keep the active contour continuous and derivable during deformation.

B. Local Gaussian Distribution fitting (LGDF)

The energy functional of LGDF is defined as follow [14]:

$$\begin{aligned} &J_{LGDF}(\phi, F_1, F_2, \sigma_1^2, \sigma_2^2) = \\ &-\beta_1 \int_\Omega \int K_\sigma(\boldsymbol{x}-\boldsymbol{y})\, p_{1,x}(u(\boldsymbol{y}))\, M_{1,\varepsilon}(\phi(\boldsymbol{y}))\, d\boldsymbol{y}\, d\boldsymbol{x} \\ &-\beta_2 \int_\Omega \int K_\sigma(\boldsymbol{x}-\boldsymbol{y})\, p_{2,x}(u(\boldsymbol{y}))\, M_{2,\varepsilon}(\phi(\boldsymbol{y}))\, d\boldsymbol{y}\, d\boldsymbol{x} \\ &+ B(H,\phi,\boldsymbol{x}) \end{aligned} \tag{11}$$

where β_1 and β_2 are two constant coefficients. Also, $p_{i,x}(u(\boldsymbol{y}))$ denotes the Gaussian PDF given by:

$$p_{i,x}(u(\boldsymbol{y})) = \frac{1}{\sqrt{2\pi}\sigma_i(\boldsymbol{x})} \exp\left(-\frac{\left(F_i(\boldsymbol{x}) - u(\boldsymbol{y})\right)^2}{2\sigma_i^2(\boldsymbol{x})}\right) \tag{12}$$

where $F_i(\boldsymbol{x})$ and $\sigma_i^2(\boldsymbol{x})$ are the average and variance of the local intensity information, respectively, for the inside ($i=1$) and outside ($i=2$) regions of the active contour. They can be optimally computed as follows:

$$F_i(\boldsymbol{x}) = \frac{\int K_\sigma(\boldsymbol{x}-\boldsymbol{y}) u(\boldsymbol{y}) M_{i,\varepsilon}(\phi(\boldsymbol{y}))\, d\boldsymbol{y}}{\int K_\sigma(\boldsymbol{x}-\boldsymbol{y}) M_{i,\varepsilon}(\phi(\boldsymbol{y}))\, d\boldsymbol{y}} \tag{13}$$

$$\sigma^2{}_i(\boldsymbol{x}) = \frac{\int K_\sigma(\boldsymbol{x}-\boldsymbol{y})(F_i(\boldsymbol{x}) - u(\boldsymbol{y}))^2 M_{i,\varepsilon}(\phi(\boldsymbol{y}))\, d\boldsymbol{y}}{\int K_\sigma(\boldsymbol{x}-\boldsymbol{y}) M_{i,\varepsilon}(\phi(\boldsymbol{y}))\, d\boldsymbol{y}} \tag{14}$$

Again, the first two terms of (11) conduct the active contour toward the desired boundary and the last expression includes some regulator terms.

IV. PROPOSED METHOD

Generally, it seems that the global Gaussian PDF is well suited to images with piecewise-constant regions [8, 19]. Hence, it cannot effectively take account of local intensity variations of the endo-epicard boundaries due to severe inhomogeneity.

In contrast, patch-based active contours can essentially drive intensity inhomogeneity because of using local kernels. Therefore, in the proposed method, we substitute Gaussian–based terms of the energy functional of Li's method with the local kernel-based terms of LBF and LGDF.

In more detail, it is suggested that the first term ($J_1(\phi)$) of the energy functional of the endocard active contour is substituted with the first two terms of J_{LBF} as follows:

$$\begin{aligned} &J_{endocard}(\phi_1, f_1, f_2) = \\ &\lambda_1\Big(\alpha_1 \int_\Omega \int K_{\sigma_{en}}(\boldsymbol{x}-\boldsymbol{y}) |u(\boldsymbol{y}) - f_1(\boldsymbol{x})|^2 M_{1,\varepsilon}\, d\boldsymbol{y}\, d\boldsymbol{x} + \\ &\alpha_2 \int_\Omega \int K_{\sigma_{en}}(\boldsymbol{x}-\boldsymbol{y}) |u(\boldsymbol{y}) - f_2(\boldsymbol{x})|^2 M_{2,\varepsilon}\, d\boldsymbol{y}\, d\boldsymbol{x}\Big) + \\ &\lambda_2 J_2(\phi_1) + \lambda_3 J_3(\phi_1) + \lambda_4 J_4(\phi_1) \end{aligned} \tag{15}$$

where ϕ_1 is the level set function of the endocard active contour. Considering the Euler-Lagrange equation, the endocard active contour should deform according to the following differential equation:

$$\frac{\partial \phi_1}{\partial t} = \left[\lambda_1(\alpha_2 e_2 - \alpha_1 e_1) - A(\phi_1, t)\right]\delta(\phi_1) \tag{16}$$

where e_1 and e_2 are given by:

$$\begin{cases} e_1(\boldsymbol{x}) = \int_\Omega K_{\sigma_{en}}(\boldsymbol{y}-\boldsymbol{x}) \left| u(\boldsymbol{x}) - f_1(\boldsymbol{y})\right|^2 d\boldsymbol{y} \\ e_2(\boldsymbol{x}) = \int_\Omega K_{\sigma_{en}}(\boldsymbol{y}-\boldsymbol{x}) \left| u(\boldsymbol{x}) - f_2(\boldsymbol{y})\right|^2 d\boldsymbol{y} \end{cases} \tag{17}$$

However, the epicard inhomogeneity is more severe compared to the endocard due to extreme intensity variations of the right ventricle and viscera. Therefore, for more effective inhomogeneity handling of intensity variations, we offer the usage of LGDF instead of LBF for the region-based term of the epicard energy functional as follows:

$$\begin{aligned} &J_{epicard}(\phi_2, F_1, F_2, \sigma_1^2, \sigma_2^2) = \\ &-\beta_1 \int_\Omega \int K_{\sigma_{ep}}(\boldsymbol{x}-\boldsymbol{y})\, p_{1,x}(u(\boldsymbol{y}))\, M_{1,\varepsilon}(\phi_2(\boldsymbol{y}))\, d\boldsymbol{y}d\boldsymbol{x} \\ &-\beta_2 \int_\Omega \int K_{\sigma_{ep}}(\boldsymbol{x}-\boldsymbol{y})\, p_{2,x}(u(\boldsymbol{y}))\, M_{2,\varepsilon}(\phi_2(\boldsymbol{y}))\, d\boldsymbol{y}d\boldsymbol{x} \\ &+ \lambda_3 J_3(\phi_2) + \lambda_4 J_4(\phi_2) + \lambda_5 J_5(\phi_2) \end{aligned} \tag{18}$$

In comparison with (15), the edge-based term $J_2(\phi_2)$ is discarded in the above energy functional to prevent the epicard active contour from being attracted by irrelevant edges.

Again based on the Euler-Lagrange equation, the evolution differential equation of the epicard active contour can be given by:

$$\frac{\partial \phi_2}{\partial t} = \left[\lambda_1(\beta_2 E_2 - \beta_1 E_1) - A(\phi_2, t) + \lambda_5 D\right]\delta(\phi_2) \tag{19}$$

where, E_1 and E_2 are computed by:

$$\begin{cases} E_1(\boldsymbol{x}) = \int_\Omega K_{\sigma_{ep}}(\boldsymbol{y}-\boldsymbol{x}) \left[\log(\sigma_1(\boldsymbol{y})) + \dfrac{\left(F_1(\boldsymbol{y}) - u(\boldsymbol{x})\right)^2}{2\sigma_1^2(\boldsymbol{y})}\right] d\boldsymbol{y} \\ E_2(\boldsymbol{x}) = \int_\Omega K_{\sigma_{ep}}(\boldsymbol{y}-\boldsymbol{x}) \left[\log(\sigma_2(\boldsymbol{y})) + \dfrac{\left(F_2(\boldsymbol{y}) - u(\boldsymbol{x})\right)^2}{2\sigma_2^2(\boldsymbol{y})}\right] d\boldsymbol{y} \end{cases} \tag{20}$$

V. EXPERIMENTAL RESULT AND EVALUATION

Ten different CMR images were chosen from the LAAV database [20] to evaluate the performance of the proposed algorithm compared to Li's method. In all

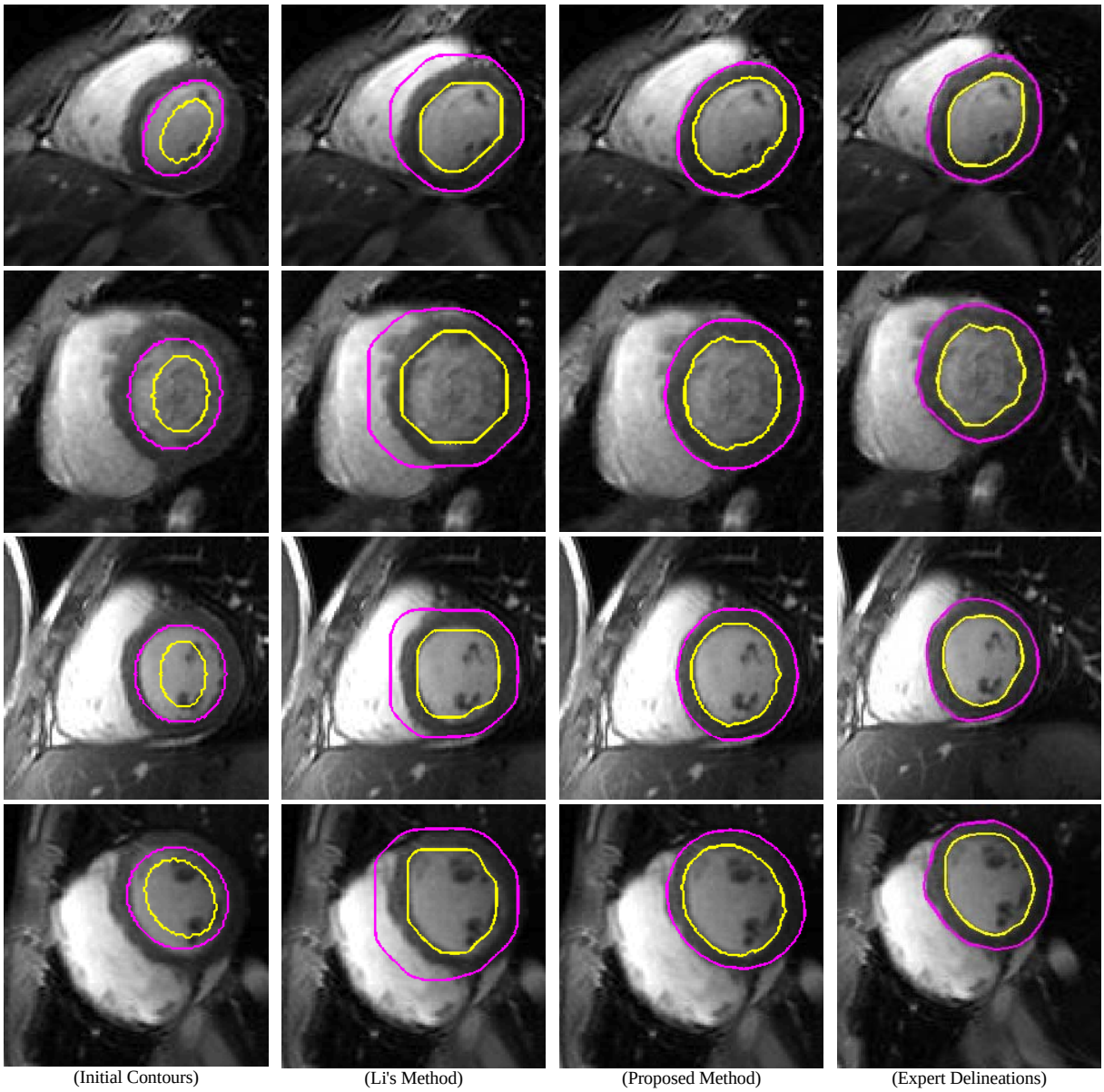

(Initial Contours) (Li's Method) (Proposed Method) (Expert Delineations)

Figure 1. Comparing the results of the proposed active contour and Li's method with manually delineated boundaries provided by an expert for four different CMR images.

TABLE I. COMPARING THE RESULTS OF THE PROPOSED ALGORITHM WITH THOSE OF LI'S METHOD FOR 10 BENCHMARK CMR IMAGES IN TERMS OF THE AREA-SIMILARITY AND SHAPE-SIMILARITY MEASURES. THE BEST RESULTS ARE INDICATED BY BOLD-FACED TEXT.

Subject	S_{area}		S_{shape} **for Endocard Boundary**		S_{shape} **for Epicard Boundary**	
	Li's Method	*Proposed*	*Li's Method*	*Proposed*	*Li's Method*	*Proposed*
1	0.77	**0.86**	0.66	**0.84**	0.67	**0.85**
2	0.77	**0.85**	0.86	**0.91**	0.56	**0.79**
3	0.71	**0.88**	0.73	**0.97**	0.5	**0.84**
4	0.69	**0.89**	0.80	**0.82**	0.49	**0.95**
5	0.67	**0.88**	0.62	**0.93**	0.42	**0.87**
6	0.66	**0.89**	0.85	**0.93**	0.40	**0.91**
7	0.56	**0.86**	0.81	**0.94**	0.38	**0.96**
8	0.69	**0.85**	0.82	**0.91**	0.62	**0.91**
9	0.72	**0.90**	**0.95**	**0.95**	0.51	**0.95**
10	0.77	**0.86**	**0.97**	0.96	0.67	**0.97**
Average (STD)	0.70 (0.06)	**0.87** (0.02)	0.81 (0.11)	**0.92** (0.05)	0.52 (0.11)	**0.90** (0.06)

benchmark images (with the size of 256×256 pixels), the endo-epicard boundaries were manually delineated by an expert.

A. Parameters Adjustment

In all experiments, the algorithm parameters were experimentally adjusted as $\alpha_1=\alpha_2=10^4$, $\beta_1=4$, $\beta_2=2$, $\sigma_{en}=0.25$, and $\sigma_{ep}=5$. The coefficient λ_4 is also set to 100 and 10 for endocard and epicard active contours, respectively.

Furthermore, the coefficients λ_1, λ_2, and λ_5 were further regulated according to the cooling phase of the approach originally presented by Chen *et al* [11] as follows:

$$\lambda_i(n)=\frac{1}{2}[\lambda_i(0)-\lambda_i(N)]\left[1+\cos(\frac{n\pi}{N})\right] \quad i=1,2,5 \qquad (21)$$

where n is the iteration counter and N represents the total number of iterations. Besides, in the same manner, λ_3 was attuned as follows:

$$\lambda_3(n)=\frac{\lambda_3(N)-\lambda_3(0)}{\cosh[10-(\frac{n}{N}-1)]}+\lambda_3(0) \qquad (22)$$

The initial and final values of λ_i (i=1,2,…,5) were experimentally chosen as $[\lambda_1(0)=2,\lambda_1(N)=0.2]$, $[\lambda_2(0)=2\times10^3,\lambda_2(N)=0]$, and $[\lambda_3(0)=0,\lambda_3(N)=10^8]$ for endocard active contour. Also, in the epicard active contour, we had $[\lambda_1(0)=120,\lambda_1(N)=20]$, $[\lambda_3(0)=0,\lambda_3(N)=80]$, and $[\lambda_5(0)=140,\lambda_5(N)=40]$.

Finally, it is worth to cite that in all experiments, the same parameters values were used with N=150.

B. Evaluations

In Fig. 1, the results of the proposed active contour and Li's method are compared with expert delineations for four CMR images. The proposed algorithm successfully extract both the endocard and epicard boundaries in all benchmark images although Li' method partially failed to segment the epicard boundary.

For further quantitative comparisons, we used the area-similarity (S_{area}) and shape-similarity (S_{shape}) measures [9]. In more detail, the area-similarity measure ($S_{\text{area}} \in [0,1]$) compares the myocardium region (A_1) obtained by a counterpart algorithm with the manually segmented area (A_2), as follows:

$$S_{\text{area}}=\frac{2\,n(A_1 \cap A_2)}{n(A_1)+n(A_2)} \qquad (23)$$

where $n(.)$ returns the number of pixels in a region.

However, S_{area} cannot effectively evaluate the shape of the resultant endocard and epicard boundaries compared to those of the manual delineation. To address this problem, we also used the shape-similarity measure proposed by Pluempitiwiriyawej *et al* [9]. For two completely matched curves, S_{shape} results to 1 while it decreases to 0 in the worst case.

The results are presented in Table I. As shown, the proposed active contour provided the best results for most CMR images. In more detail, compared to Li's method, it improved the average area-similarity measure by 17%. Furthermore, the average shape-similarity of the proposed algorithm is superior to Li's method by 10% and 38% for endocard and epicard boundaries, respectively. Obviously, Li's method provided poor results for the epicard boundary, mainly, due to severe intensity inhomogeneity while the proposed approach appropriately tackled this problem by using the localized patch-based energy functional.

VI. CONCLUSION

This paper presented a new active contour for segmentation of the myocardium of the left ventricle in CMR images. We experimentally found out that the region-based term of STACS and its variants such as Li's method could not effectively drive the intensity inhomogeneity of the endocard and, especially, epicard boundaries. Thus, the original region-based term of Li's method was substituted with two separate patch-based expressions, derived from LBF and LGDF. The experimental results demonstrated superior performance of the presented active contour compared to Li's method for a number of inhomogeneous CMR images. It provided better results for both endocard and epicard boundaries in terms of area-similarity and also, shape-similarity measures.

REFERENCES

[1] G. Hautvast, Segmentation of short axis cardiac MR using active contours. M.Sc. thesis, University of Eindhoven, 2004.

[2] C. Petitjean, J.N Dacher, “A review of segmentation methods in short axis cardiac MR images”, Medical Image Analysis, vol. 15, no. 2, pp. 169-184, 2011.

[3] S. Ranganath, “Contour extraction from cardiac MRI studies using snakes”, IEEE. Trans. Med. Imag, vol. 14, no. 2, pp. 328–338, 1995.

[4] I.Ben Ayed, S. Li, I. Ross, “Embedding overlap priors in variational left ventricle tracking”, IEEE Trans. Med. Imag, vol. 28, no. 12, pp. 1902–1913, 2009.

[5] M. Lynch, O. Ghita, and P. F. Whelan “Left-ventricle myocardium segmentation using a coupled level-set with a priori knowledge,” Computerized Medical Imaging and Graphics, vol. 30, no. 4, pp. 255–262, 2006.

[6] S. Kichenassamy, A. Kumar, P. Olver, A. Tannenbaum, and A. Yezzi, “Conformal curvatures flows: From phase transitions to active vision,” Archive and Rational Mechanics for Analysis, vol. 134, no. 3, pp. 275–301, 1996.

[7] J. Woo, B.-W. Hong, A. Ramesh, G. Germano, C.-C. Jay Kuo, and P. Slomka, “Curve Evolution with A Dual Shape Similarity and Its Application to Segmentation of Left Ventricle,” Medical Imaging: Physics of Medical Imaging .Proc. of SPIE, vol. 7259, pp. 7259T_1, 2009.

[8] T. Chan and L. Vese, “Active contours without edges,” IEEE Trans. Image Processing, vol. 10, no. 2, pp. 266–277, 2001.

[9] C. Pluempitiwiriyawej, J. M. F. Moura, Y.-J. Lin Wu, C. Ho, “STACS: New active contour scheme for cardiac MR image segmentation,” IEEE Trans. Medical Imaging, vol. 24, no. 5, pp. 593–603, 2005.

[10] A. Schöllhuber, Automatic segmentation of contrast enhanced cardiac MRI for myocardial perfusion analysis. M.Sc. Thises, Inst. Comp. Graph. Alg, Vienna Univ, Vienna, Austria, 2008.

[11] T. Chen, J. Babb, P. Kellman, L. Axel, and D. Kim, “Semiautomated segmentation of myocardial contours for fast

strain analysis in cine displacement-encoded MRI," IEEE Trans. Medical Imaging, vol. 27, no. 8, pp. 1084–1094, 2008.

[12] C. Li, X. Jia, and Y. Sun, "Improved semi-automated segmentation of cardiac CT and MR images," IEEE Int'l Symp. Biomedical Imaging: From Nano to Macro, pp. 25 - 28, 2009.

[13] C. Li, C. Kao, J. Gore, and Z. Ding, "Minimization of region-scalable fitting energy for image segmentation," IEEE Trans, Image Processing, vol. 17, no. 10, pp. 1940–1949, 2008.

[14] L. Wang, L. He, A. Mishra, and C. Li, "Active contours driven by local Gaussian distribution fitting energy," Signal. Processing, vol. 89, no. 12, pp. 2435–2447, 2009.

[15] S. Lankton and A. Tannenbaum, "Localizing region-based active contours," IEEE Trans. Image Processing, vol. 17, no. 11, pp. 2029–2039, 2008.

[16] K. Zhang, H. Song, and L. Zhang, "Active contours driven by local image fitting energy," J. of Pattern Recognition, vol. 43, no. 4, pp. 1199–1206, 2010.

[17] C. Li, R. Huang, Z. Ding, C. Gatenby, D. N. Metaxas, and J. C. Gore, "A level Set method for image segmentation in the presence of intensity inhomogeneities with application to MRI," IEEE Trans. Image Processing, vol. 20, no. 7, pp. 2007–2016, 2011.

[18] Yuan, J. and Li, P. and Wen, Y. and Xu, Y, "Level set segmentation of intensity inhomogeneous images based on local linear approximation of difference image", IET Image Processing, vol. 6, no. 5, pp. 473-482, 2012.

[19] L. Vese and T. Chan, "A multiphase level set framework for image segmentation using the Mumford and Shah model," Int'l Journal of Computer Vision, vol. 50, no. 3, pp. 271–293, 2002.

[20] J. Tsotsos, "Laboratory for Active and Attentive Vision (LAAV)". [Online] Available: http://www.cse.yorku.ca/~mridataset/